

A global albedo data set derived from AVHRR data for use in climate simulations

Nicholas C. Strugnell¹

Department of Geography, Boston University, Boston, Massachusetts

Wolfgang Lucht

Potsdam-Institut für Klimafolgenforschung, Potsdam, Germany

Crystal Schaaf

Department of Geography, Boston University, Boston, Massachusetts

Abstract. We present a global 1-km albedo dataset derived from Advanced Very High Resolution Radiometer (AVHRR) satellite remote sensing data, a global land cover classification and field observations of typical land surface bidirectional reflectance distribution functions (BRDFs). There is a clear need for such a global albedo map for use in atmospheric radiative transfer models. A land cover classification based on surface structure is employed and class correspondences used to generate a structural class map from an existing ecological global land classification. Representative field measurements of BRDF are assigned to each of the structural classes allowing us to retrieve BRDF shape parameters and albedo for each class using a semiempirical model. These parameters were adjusted using global AVHRR data to account for intra-class variations of surface reflectance. Albedos were calculated from the adjusted parameters and summarised by land cover type, continent and season.

Introduction

A previous article [Strugnell and Lucht, 2000] describes a method to derive land surface albedos from satellite-sensed bidirectional reflectances. Directional reflectances were used to constrain an estimate of the BRDF of the underlying surface and the resulting modified function integrated to produce the albedo. In this paper, we describe how the research has been expanded to retrieve albedos over the global land surface.

Reflectance to Albedo Transformation

The directional reflectance of a surface can be expressed as a function of illumination and observation angles, known as the BRDF. The black-sky albedo (directional-hemispherical reflectance) is obtained by integrating over the observational hemisphere and is a function of solar zenith angle. The BRDF, a differential quantity, cannot be directly measured. Instead we may *sample* it through the measurement of bidirectional reflectance factors (BRFs): the ratio of radiance reflected by a target surface to that reflected by a

Lambertian panel. Under clear sky conditions, and for a sensor with a sufficiently small field of view, the BRF is approximately equal to π times the point value of the BRDF. To retrieve the continuous BRDF from BRF measurements, an invertible model is required. For this study we used the RossThick-LiSparseModis Reciprocal (RTLSPMR) model [Lucht *et al.*, 2000]. The model describes BRDF as the weighted sum of two functions of the viewing and illumination angles, and a constant value. The model is used to calculate directional reflectances given these three weights (the forward mode) or to calculate the weights and hence the shape of the BRDF given a set of directional observations (the inverse mode.)

In Strugnell and Lucht [2000] we proposed an albedo retrieval method for situations in which as few as one directional reflectance observation is available. The method uses *a priori* knowledge of surface BRDFs to compensate for the lack of directional information in the observations. A land cover classification based on surface structure was generated from the Olson classification [Olson, 1994] map produced by Loveland *et al.* [1999]. Structural maps are dynamic in that the mapping between an ecological class and a structural class is not fixed. Rather, the mapping varies according to season since the structure of a given ecological class is dependent on whether the canopy is in leaf or senescent and on the presence or absence of snow. For example, a forest stand in New England might be statically classified as *deciduous broadleaf forest* under the Olson system. Under the structural system such a stand would be classified as *dense broadleaf trees/shrubs* in summer, *dense senescent broadleaf trees/shrubs* in winter and *dense senescent broadleaf trees/shrubs on snow* following a snow fall.

The BRDF of a land cover class, varies from one location to another. It is fair to assume however that intra-class BRDFs are broadly similar and that differences are one of degree, rather than substantial changes in the shape of the function. We further this by grouping within classes land cover types that theory and measurement suggest will have similar BRDFs. Thus *boreal needleleaf forest* and *Mediterranean needleleaf forest*, which occupy different classes in the Olson scheme, occupy the same classes in the structure-based scheme.

We associate surface BRDFs with each class of the structural classification. These BRDFs are retrieved from densely

¹Now at ArsDigita Ltd, London, UK

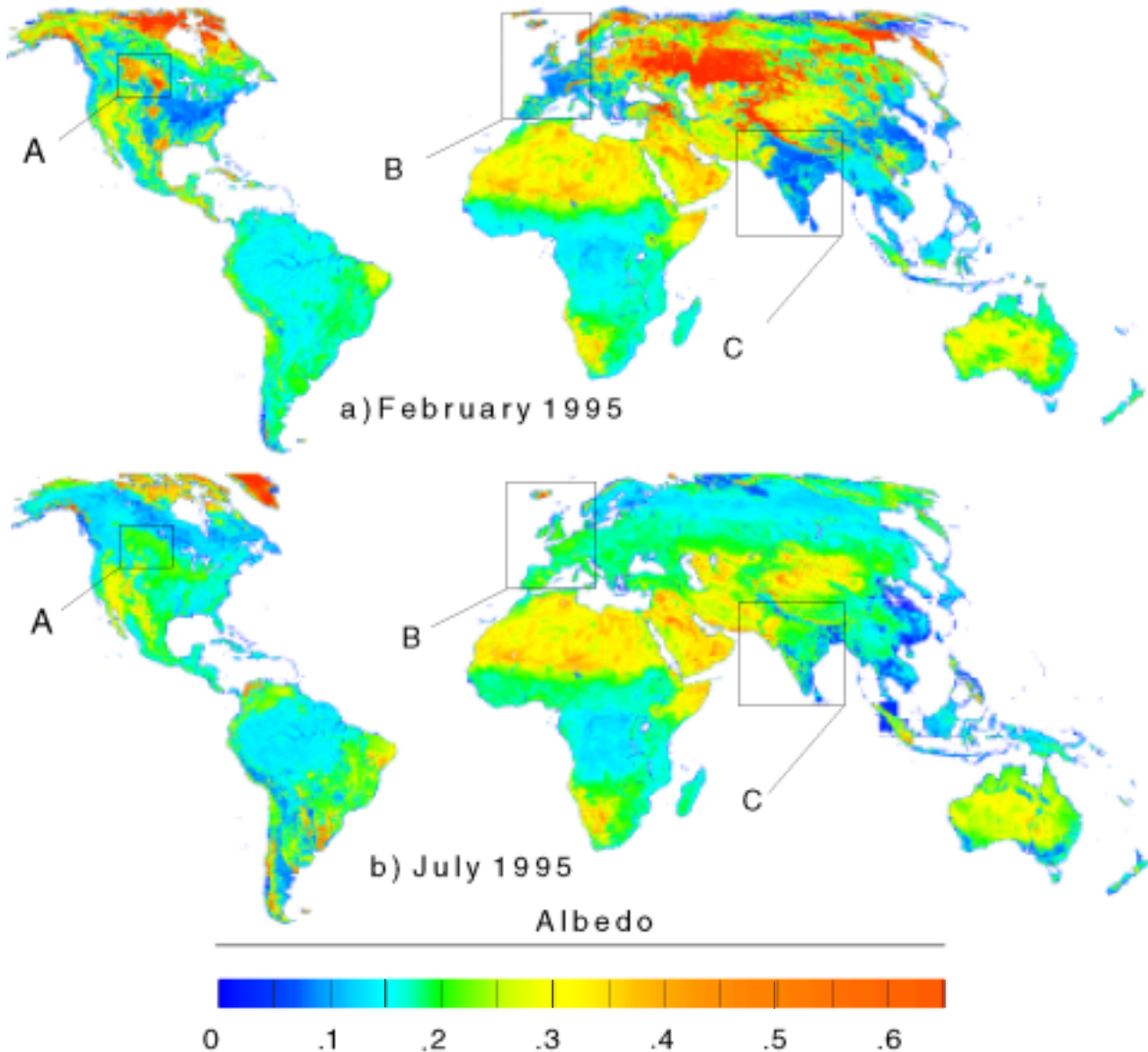


Plate 1. Global broadband (350–3000nm) local solar noon black-sky surface albedos from February and July 1995 AVHRR data.

sampled measurements of surface directional reflectances, principally from ground-based (and some airborne) instruments. The BRDFs are expressed in terms of the three weights of the RTLSMR model. These measured BRDFs were chosen to represent a consensus surface for the structural class under consideration. For this reason we term them *archetype* BRDFs. The archetype BRDF represents a typical surface within the range of possibilities represented by the structural class.

By introducing remotely sensed data we can account for intra-class variation in the BRDF by simply adjusting the archetype BRDF to fit the AVHRR observations. We proposed that the local BRDF of the surface, $R_r(\Omega_i; \Omega_r)$, be modelled as a function of the archetypal BRDF, $R_a(\Omega_i; \Omega_r)$ using a simple multiplicative factor a :

$$R_r(\Omega_i; \Omega_r) = a \cdot R_a(\Omega_i; \Omega_r). \quad (1)$$

We justify the use of a multiplicative factor, a , to generate a family of similar BRDFs from one archetype by considering

the changes in directional effects as the overall brightness of a scene changes. As scene brightness increases we tend to see an increase in directional effects: the typical bowl or inverted bowl-shape of the BRDF becomes more pronounced as the albedo increases. Conversely, as the overall scene brightness decreases we see a reduction of the directional effects. The phenomenon can be simply explained by noting that a bright scene tends to have a higher contrast between vegetation canopy and soil background which leads to a more non-Lambertian BRDF. A dark scene will tend to have little contrast in it and hence a weaker BRDF effect. This arises because an important component of reflectance anisotropy is caused by the interaction of dark shadows on bright backgrounds; if there is little contrast in the scene, the shadowing process has little effect. Secondly, BRDF effects which originate from radiative transfer within a vegetation canopy, are more pronounced when absorption is low, and low absorption is associated with high scene brightness. For values of a close to unity we expect a multiplicative factor

to reproduce this behaviour: as the multiplier increases, reflecting an increase in overall scene brightness, the BRDF effect will increase. Using the multiplicative factor we may define a family of BRDF shapes associated with each land cover class, each member of that family being produced by varying a .

We determine a on a per-band basis by a least squares minimisation of the difference between directional reflectances predicted by the archetypal BRDF, and those actually measured by the AVHRR sensor. The predicted measurements are found by running the RTLSMR model in the forward mode using the archetypal BRDF under the same view and illumination angles as the AVHRR measurements available.

As in all comparisons of remotely-sensed data and ground measurements the issue of scaling artifacts must be addressed. This is particularly the case in this study where ground-based measurements of BRDF, typically at scales of 10–200 m, are used in combination with 1 km satellite data. The BRDF of a homogeneous land surface is constant at any scale substantially larger than scene elements - a few metres for a grassland, or a few tens of metres for a forest. Sub-pixel inhomogeneity, for example the mixed agricultural pattern typical of densely populated countries, leads to changes in BRDF retrieval results with increasing scale as noted in *Muller and Disney* [1996]. Confidence in albedos ascribed to inhomogeneous areas should therefore be reduced.

Broadband Transformation

BRDFs in the relatively narrow wavebands of satellite sensors need to be converted to broader bands of utility to climatologists. With each BRDF class we associate a reflectance spectrum from the ASTER spectral library [*Hook et al.*, 1998]. We expect the local reflectance of ground pixels within each BRDF class to broadly follow these reflectance spectra, with some variation in overall brightness and contrast between the visible and NIR. We therefore propose that we can express the local spectrum, $\rho_s(\lambda)$ as a linear transformation of the library spectrum, $\rho_l(\lambda)$:

$$\rho_s(\lambda) = A \cdot \rho_l(\lambda) + B. \quad (2)$$

This simple transformation approximates the variability in the reflectance spectra of both vegetated and non-vegetated surfaces quite well. In the case of non-vegetated soils the offset term, B , accounts for differences in overall brightness, while the scaling term, A , accounts for the contrast between visible and SWIR reflectances in vegetated surfaces.

A reflectance measurement over the range λ_a, λ_b samples $\rho_s(\lambda)$ as follows:

$$\rho_0 = \frac{\int_{\lambda_a}^{\lambda_b} \rho_s(\lambda) d\lambda}{\lambda_b - \lambda_a}, \quad (3)$$

Using AVHRR bands 1 and 2, and a known library spectrum

we use Eqn 3 to solve for A and B in Eqn 2. Equipped with the local spectrum, $\rho_s(\lambda)$, we can calculate BRDF factors over an arbitrary spectral interval λ'_a, λ'_b by convolving the local spectrum with a bottom of atmosphere solar irradiance spectrum. In *Strugnell and Lucht* [2000], this method of broadband conversion is shown to be accurate to within

10% when used to convert AVHRR-derived measurements to total shortwave broadband values.

Results and Discussion

We derived global BRDF datasets at a 1 km resolution from 30 day maximum value composite AVHRR data from February and July 1995. The compositing process leads to a single reflectance observation so the least squares minimisation procedure simplifies to $a = \frac{\rho_r}{\rho_a}$ where ρ_r and ρ_a are the measured and predicted reflectances. The broadband transformation was also applied to retrieve BRDF parameters in the broad visible (350–680 nm), infrared (680–3000 nm) and fullband (350–3000 nm). We calculated black-sky albedos at local solar noon from the BRDF parameters using the parameterisation given in *Lucht et al.* [2000].

Plate 1 shows the fullband black-sky albedo for February and July 1995. The February image is truncated at the top due to the low sun angle. Albedo is scaled identically in both maps which are in the Goode's projection.

Area A in Plate 1 consists principally of mid latitude steppe. The area has a high albedo in the July scene due to the very high NIR reflectance of growing cereal crops and grass. In the February scene the albedo is even higher as the grass is by now covered in snow. By contrast, the remainder of North America below the Great Lakes shows an overall reduction in albedo. This area consists of deciduous and mixed forest and cropland mosaics. Although it is likely that there is snow on the ground in this area in the February scene, it is partially obscured by the canopy.

Area B contains mainly forest and crop mosaics and shows a similar lowering of albedo from July to February. The exceptions are the mountain chains of the Alps and Scandinavia and the lowlands of eastern Great Britain and the Low Countries which, like the North American Great Plains do not have enough of an overstory canopy to obscure snowfall. Snow brightening is also obvious in the February scene across central Asia into the Tibetan Plateau and Siberia.

In area C we see a distinct lowering in albedo from July to February, much as we might see in the temperate zones. The increase in albedo in July is due to the effects of the southwest Monsoon that brings rain to the subcontinent in June. This causes a green-up of vegetation which increases the broadband albedo. By contrast, February is at the end of the weak northeast Monsoon which brings dry air from central Asia resulting in drought and a consequent reduction of greenness, and hence albedo, across the continent. The area of near-constant albedo in the northeast corner of the area of interest is the Great Indian Desert.

Summarised Snow-free Albedos

summarises mean albedos by International Geosphere-Biosphere Programme (IGBP) class. The IGBP classification [*Loveland et al.*, 1999] is designed to be of utility to both the climate modelling and ecological communities and has been chosen as the principal classification system of the MODIS land cover product. The IGBP map here used is that of *Loveland et al.* [1999]. We have attempted to exclude all areas under snow and ice by using a threshold reflectance of 0.65 in both AVHRR channels, as snow and ice areas would have greatly exaggerated the February albedos for the northern continents. This technique does not detect

Table 1. Broadband black-sky albedos summarised by continent and month. IGBP classes are as follows: **1** Evergreen Needleleaf Forest, **2** Evergreen Broadleaf Forest, **3** Deciduous Needleleaf Forest, **4** Deciduous Broadleaf Forest, **5** Mixed Forest, **6** Closed Shrublands, **7** Open Shrublands, **8** Woody Savannas, **9** Savannas, **10** Grasslands, **11** Permanent Wetlands, **12** Croplands, **13** Urban and Built-Up, **14** Cropland/Natural Vegetation Mosaic, **15** Snow and Ice, **16** Barren or Sparsely Vegetated. Continents are as follows: **A** Africa north of Equator, **B** Africa south of Equator, **C** Australasia, **D** Eurasia, **E** North America, **F** South America.

IGBP Class	February 1995						July 1995					
	A	B	C	D	E	F	A	B	C	D	E	F
1	—	—	—	0.299	0.185	—	—	—	—	0.139	0.135	—
2	0.137	0.143	0.080	0.141	0.151	0.154	0.141	0.141	0.150	0.146	0.160	0.143
3	—	—	—	0.229	—	—	—	—	—	0.142	—	—
4	—	0.134	0.147	0.176	0.133	0.154	—	0.128	0.174	0.175	0.159	0.152
5	—	—	0.140	0.198	0.178	0.140	—	—	0.179	0.151	0.139	0.226
6	0.292	—	0.129	0.268	0.226	0.229	0.298	—	0.154	0.228	0.135	0.219
7	0.350	0.326	0.308	0.271	0.303	0.211	0.344	0.347	0.283	0.270	0.271	0.196
8	0.160	0.151	0.157	0.198	0.277	0.162	0.174	0.141	0.193	0.167	0.171	0.179
9	0.188	0.177	0.212	0.190	0.180	0.167	0.189	0.179	0.248	0.190	0.215	0.200
10	0.248	0.220	0.208	0.232	0.170	0.173	0.242	0.234	0.187	0.216	0.199	0.135
11	0.146	0.159	0.278	0.260	0.322	0.175	0.167	0.173	0.164	0.167	0.149	0.188
12	0.182	0.169	0.156	0.178	0.198	0.275	0.180	0.177	0.145	0.158	0.184	0.132
13	0.178	0.181	0.168	0.228	0.177	0.181	0.181	0.192	0.170	0.176	0.193	0.201
14	0.188	0.173	0.151	0.216	0.213	0.175	0.194	0.172	0.139	0.179	0.187	0.195
15	—	—	—	—	—	—	—	—	—	—	—	—
16	0.316	0.273	0.334	0.302	0.161	0.221	0.322	0.263	0.262	0.316	0.273	0.214

the effects of snow lying under trees which causes an unexpected elevation in the albedo of some classes in February *e.g.* evergreen needleleaf forest.

This summary of local noon black-sky albedos results in the aggregation of pixels under differing solar zenith angles and readers who are interested in albedos summarised by latitudinal zones should contact the authors. The results in Table show some agreement with the values published in Table 4 of *Henderson-Sellers and Wilson*[1983], however the current results show larger seasonal differences than that study. In the northern hemisphere, increased albedos in February are caused by inadequate snow masking; this is apparent for class 1 in Table . Inadequate cloud masking may also be responsible for artificially high albedos in Central America. The substantial regional changes in albedo described in the previous section, however, reflect real changes in surface structure occasioned by changes in vegetation. The spatial patterns of albedo in Plate 1 are also in agreement with the global datasets summarised in *Csiszar and Gutman*[1999.]

Acknowledgments. This work was funded through JPL subcontract 960916/97 and EOS-MODIS grant NAS5-31369. W. Lucht was supported under BMBF (Germany) project 01LA9828/0. We gratefully acknowledge the PI of this project, Ralph Kahn, Alan Strahler for support in Boston, ArsDigita, and two anonymous referees.

References

Csiszar, I. and G. Gutman, Mapping global land surface albedo from NOAA AVHRR, *J. Geophys. Res.*, 104, D6, 6215–6228, 1999.

Henderson-Sellers, A. and M. F. Wilson, Surface albedo data for climatic modeling, *Rev. Geophys. and Space Phys.*, 21, 8, 1743–1778, 1983.

Hook, S. J., J. Salisbury and C. I. Grove, The ASTER spectral library, CD-ROM, Jet Propulsion Laboratory, Pasadena, Ca., 1998.

Loveland, T. R., Z. L. Zhu, D. O. Ohlen, J. F. Brown, B. C. Reed, and L. Yang, The IGBP-DIS global 1-km land-cover data set DISCover: A project overview, *Photogramm. Eng. Remote Sens.*, 9, 1013-1020, 1999.

Lucht, W., A. H. Strahler and C. B. Schaaf, An algorithm for the retrieval of albedo from space using semiempirical BRDF models, *IEEE T. Geosci. Rem. Sens.*, 38, 2, 977–998, 2000.

Muller, J.-P. and M. Disney, ASAS scaling experiments for BRDF model inversion, *MODIS BRDF/Albedo Product: Algorithm Theoretical Basis Document Version 4.0*, NASA Technical Report, 1996.

Olson, J. S., Global ecosystem framework—definitions, 37pp., Internal Report, USGS EROS Data Center, Sioux Falls, So. Dakota, 1994.

Strugnell, N. C. and W. Lucht, Continental-scale albedo inferred from AVHRR data, land cover class and field observations of typical BRDFs, *J. Clim.*, In Press, 2000.

N. C. Strugnell, ArsDigita Ltd, 42 Brook St, London, W1Y 1YB, UK. (e-mail: nstrug@arsdigita.com)

C. Schaaf, Dept of Geography, Boston University, 675 Commonwealth Ave, Boston, MA 02215-1401. (e-mail: schAAF@bu.edu)

W. Lucht, PIK, Telegrafenberg C4, Postfach 60 12 03, D-14412 Potsdam, Germany. (e-mail: wlucht@pik-potsdam.de)

(Received February 9, 2000; revised August 15, 2000; accepted September 8, 2000.)